IEEE Transactions on Nuclear Science, Vol. NS-34, No. 6, December 1987

THE SIZE EFFECT OF ION CHARGE TRACKS ON SINGLE EVENT MULTIPLE-BIT UPSET*

R. C. Martin and N. M. Ghoniem
Mechanical, Aerospace and Nuclear Engineering Department
University of California, Los Angeles, CA 90024

Y. Song and J. S. Cable
TRW Inc.
One Space Park, Redondo Beach, CA 90278

ABSTRACT

Double-bit upset rates in satellite memory cells as high as several percent of total upsets have recently been reported. This significant fraction may be explained by cosmic ion track sizes which are larger than previously postulated. Generation and transport of high-energy secondary electrons along heavy-ion tracks have been analyzed using the Monte Carlo (MC) code TRIPOS-E. Indications are that initial track radii are significantly larger than previously thought. In this paper, an evaluation of the probability of double-bit upsets as a function of track size and hypothetical device dimensions is presented.

INTRODUCTION

A high ratio of multiple to single-bit upset rates over a two-year period has been reported on a satellite subsystem containing Harris HM-6508 CMOS RAMs. The rate of double-bit upsets in adjacent memory cells is believed to be 5% to 10% that of single-bit upsets [1]. The probability of these multiple upsets being caused by consecutive hits from cosmic rays has been determined to be negligibly small. Similar experiences with bipolar RAMs, 93L422, have been reported recently [2]. In this case, the ratio of double-bit to single-bit upsets was estimated to be slightly above 1%.

Such high multiple-upset rates can pose a significant problem for single event upset (SEU) mitigation techniques, which are based on error detection and correction. For a 16-bit word, 6 extra bits are required for single-bit error detection and correction. A double-bit error in one word requires several additional bits for detection and correction. A simpler solution to double-bit error correction is the use of redundant memory cells. Neither solution is effective because of demands on circuitry, so the present approach to this problem is limited to single-bit error correction/double-bit error detection (SEC\DED). Double-bit errors within the same word can be avoided in practice by spatially dispersing those memory cells representing a single word. This solution is practical but penalties are incurred when fine geometries or high-speed operation are required.

An important parameter in SEU calculations is the initial charge track size. Numerical calculations have shown that the field lines initially confined to the depletion zone are extended to distances several times that of the depletion width. This effect gives rise to what is termed the "funneling phenomenon." Most calculations use simplified assumptions of track size and charge density. For example, a cylindrical track of 0.1 μm radius and constant excess carrier density is commonly used as the initial condition, with track generation in 1 ps [3]. A diffusion type, radially symmetric Gaussian charge distribution has also been suggested as the initial condition, with the volumetric electron-hole (e-h) pair generation along the ion path given by [4]:

$$\delta p = (N/\pi b^2) \exp(-r^2/b^2) \quad , \qquad (1)$$

with b the assumed track radius at t = 0 and N typically between 10^7 and 10^{11} e-h pairs cm^{-1}. The above approach concludes that field motion starts after the ion track expands from an initial radius of 0.1 μm to about 1 μm over 500 ps. These models may underestimate the initial charge track size because they do not take into account the range and energy deposition by energetic secondary electrons and their effect on track structure. Evidence for larger track sizes is given by cosmic ray passage through photographic emulsions, resulting in track diameters on the order of microns [5].

When an ion hits a device at an oblique angle, there is a small but finite probability of disturbing more than one sensitive junction, as shown in Fig. 1 for a hypothetical surface layer device. The larger the ion track and the closer the junctions are, the larger the probability is for upsetting more than one junction. These multiple-bit upsets will be more prevalent in fine geometry devices and with high energy ions, and will become more significant as device geometries become smaller.

This paper presents the results of a numerical study which calculates the initial charge track size of heavy ions in silicon using MC methods to analyze the slowing down of the energetic electrons produced along ion tracks. A detailed analysis is made of two ions commonly employed in cyclotron simulations of cosmic ion effects: 180 MeV argon and 270 MeV krypton. In addition, analysis is made of an iron ion with characteristics similar to those of the cosmic ray spectrum. We compare the results with an evaluation of the ratio of double- to single-bit upsets by a single ion in oblique incidence as a function of track width for typical device geometries.

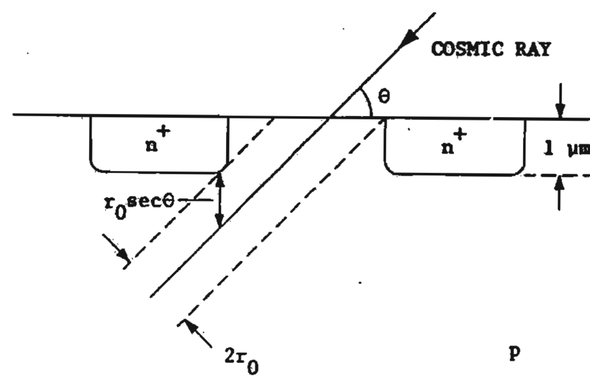

FIGURE 1. Schematic of a surface layer device, with oblique incident angle of cosmic ray causing double-bit upset. (r_0 represents the radius of the ion track.)

* Work supported by the State of California through the MICRO Project, Grant #UC-86-101, and the matching funds by TRW Corporation, #TRW-AN2700AL6S, with UCLA.

0018-9499/87/1200-1305$01.00 © 1987 IEEE

METHOD

The computer code TRIPOS was developed by Chou and Ghoniem to study ion transport in solids using the MC technique of solution of the transport equation [6]. A new version, TRIPOS-E, has recently been developed to simulate the generation and transport of secondary electrons along the ion track [7]. The electrons are generated using the binary collision approximation (BCA) and transported using an electron slowing-down subroutine following the method of Fitting and Reinhardt [8]. Electron slowing down involves both elastic and inelastic scattering, and includes core electron ionization and dielectric energy loss mechanisms. More detailed information on the implementation of the code is given elsewhere [7]. These secondary electrons, with energies on the order of several keV, can travel far from the ion track and significantly increase the track size. TRIPOS-E is capable of solving the coupled ion-electron transport problem necessary for the analysis of charge generation and track size in SEUs. In the following, we give a brief description of the new algorithm in TRIPOS-E.

Energy transfer from an ion to electrons can be represented by the Rutherford cross section:

$$d\sigma = \pi(b/2)^2\, T_{max}(dT/T^2) \quad , \qquad (2)$$

with b the impact parameter, T the kinetic energy transferred to the target particle, and T_{max} the maximum kinetic energy transferable to a target particle. In the BCA, this energy is given by:

$$T_{max} = 4m_1m_2(m_1 + m_2)^{-2}\, E \quad , \qquad (3)$$

with E the energy of the incident particle. Equation 2 shows the probability of energy transfer to be inversely proportional to the square of the transferred energy (i.e., most secondary electrons receive lower kinetic energies with a small but significant fraction receiving energies on the order of a few keV). To evaluate the distances traveled by the high energy fraction, an arbitrary cutoff energy, T_c, is used to separate the secondary electrons into two groups: those receiving kinetic energies of magnitude greater than T_c and those with energies less than T_c. T_c is typically chosen to be 0.5 to 1.0 keV. Energy transfers of magnitude greater than T_c can be viewed as discrete energy transfers to electrons. These fast electrons dissipate their energy over a significant distance from the ion path. Energy transfers of less than T_c are considered to represent continuous energy transfer, localized to e-h pairs close to the ion path. The rate of energy loss by energetic ions to electrons is given by the Bethe-Bloch equation:

$$\frac{\Delta E}{\Delta x} = \frac{\pi Z_1^2 Z_2 e^4 N}{E} \log\left[\frac{T_{max}}{T_{min}}\right] \quad , \qquad (4)$$

with Z_1 and Z_2 the atomic numbers of the incident and target atoms respectively, e the electronic charge, N the target atom density, and E the incident ion energy. T_{min} corresponds to the mean ionization energy of the target atoms, and T_{max} is given by Eq. (3). Use of T_c allows Eq. (4) to be modified to give:

$$\frac{\Delta E}{\Delta x} = C \log\left[\frac{T_{max}}{T_c}\right] + C \log\left[\frac{T_c}{T_{min}}\right] \quad , \qquad (5)$$

with C the collection of constants in Eq. (4). This equation gives the relative contributions of each energy regime to the electronic stopping of the ion. The transport and energy loss of the high-energy secondary electrons are evaluated using TRIPOS-E until their energies fall below 200 eV. Simulations of mean projected range of electrons in silicon as a function of energy give good agreement with an empirical formula [9]. The effect of varying T_c on the results was analyzed [7]. In general, extrapolation of track parameters as a function of T_c indicated lower values of T_c to give more consistent results, therefore a value of 500 eV for T_c was used in most calculations.

RESULTS

Two ions commonly used in cyclotron testing of SEU effects are studied: 270 MeV krypton and 180 MeV argon. Figure 2 gives the radial profile of a typical track for a 270-MeV krypton ion, with the endpoints of the secondary electrons plotted with respect to the ion's path. For this simulation, the endpoint is taken to be the point where the kinetic energy of the electron falls below 200 eV and T_c is taken to be 1 keV. The range of a 200 eV electron in silicon is estimated to be 69 Å [10]; with this short range and the randomized direction of electron motion, further slowing down will not alter the conclusions. The average time for these electrons to establish such a distribution is on the order of 10^{-14} s. At a depth of approximately 28 μm, the maximum energy transfer to electrons falls below the T_c value of 1 keV, in accordance with Eq. (3). Figure 2 shows that secondaries of energy greater than 1 keV can no longer be generated beyond this depth.

The secondary electrons undergo many inelastic collisions between generation and thermalization. This energy is deposited radially from the track, and e-h pair generation can be simulated by dividing the localized energy deposition by 3.6 eV, typical for generation of one e-h pair in silicon. Figure 3(a) shows the excess charge-carrier density resulting from fast electrons generated by a 270-MeV krypton ion in silicon. This is shown in the figure as a function of radial distance from the ion path at various depths of ion penetration. The carrier densities are evaluated over a 1 μm slice of silicon at each depth, with the slice perpendicular to ion motion. We define the effective track size as the distance at which the generated charge density falls below a typical silicon substrate doping (e.g., 10^{16} cm^{-3}), a region of non-equilibrium charge distribution. The effective track

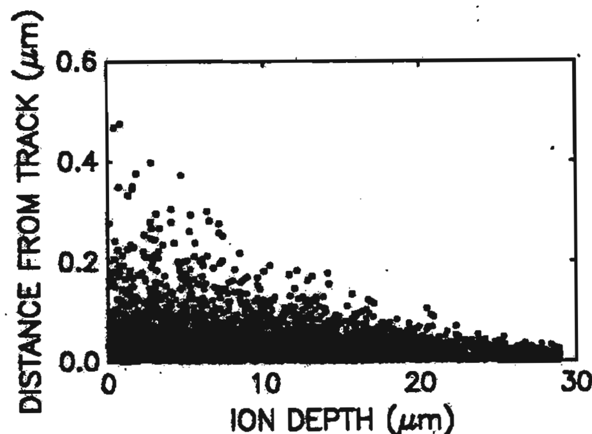

FIGURE 2. Secondary electron ranges as a function of track depth. (270-MeV krypton incident on silicon)

radius is about 0.3 μm for this krypton ion at shallow depths. A similar analysis for 180-MeV argon ions gives a radius of about 0.4 μm. The strong dependence of track radius on depth for krypton ions reflects the effect of large linear energy transfer (LET), with rapid energy loss reducing the probability of high-energy secondary-electron generation at increasing depths. The track for the lighter argon ion is wider than that of krypton because of better energy coupling with electrons, resulting in higher initial electron energies. A light ion such as a proton will generate the highest energy secondaries, but its low LET prevents significant excess carrier densities.

A similar analysis has been performed for a typical cosmic ray iron ion with energy of 0.8 GeV and LET of about 12 MeV/(mg/cm^2) in silicon. Figure 3(b) gives the radial excess carrier-density profile generated by the fast electrons for this ion at several depths of penetration. The effective radius (over which the excess carrier density exceeds a dopant concentration of 10^{16} cm^{-3}) is about 0.6 μm, well above track radii of 0.1 μm assumed in several previous SEU simulations [3,4]. The larger range of this high-energy ion relative to krypton results in more uniform excess carrier distributions over the first 20 μm of ion range than is apparent for krypton in Fig. 3(a). For krypton, the radial profiles fall off markedly with depth. Simulation of 180-MeV argon ions gave results similar to those of iron; argon's longer range relative to krypton resulted in a uniform charge profile over the first 20 μm of penetration by argon in silicon.

A significant result from these simulations, apparent in Figs. 3(a) and 3(b), is the exponential decline in excess carrier density away from the central core of the ion track. This indicates high-energy penetration by the secondary electrons. This result has not been suggested in the previous simulations of ion tracks which assume either a Gaussian or uniform charge distribution. A non-exponential regime exists close to the ion path. To account for this non-exponential regime and to include the contribution to e-h pair generation by all energy transfers less than T_c, a Gaussian-like charge distribution is assumed for the central core of the track, similar to the approach in Ref. [4]. Combining these Gaussian and exponential regimes allows derivation of an analytical expression which can be fitted to the results from TRIPOS-E:

$$\eta(r) = (C/r)[\exp(-r^2/b_1^2) + \xi \exp(-r/b_2)] \quad , \quad (6)$$

with $\eta(r)$ the radial density of the e-h pairs, C a constant, b_1 and b_2 analogous to characteristic track radii for the Gaussian and exponential regimes respectively, ξ a correlation factor between the two components, and the 1/r dependency reflecting the cylindrical geometry. Integration of the charge density over space allows evaluation of C:

$$C = \frac{N_T}{\pi^{3/2} b_1 + 2\pi\xi b_2} \quad , \quad (7)$$

with N_T the total e-h pair generation along a unit path length of the ion, proportional to the ion's LET. Given the total e-h pair generation within a region of interest and the excess carrier profiles resulting from the high-energy secondary electrons as in Figs. 3(a) and 3(b), the parameters b_1, b_2, and ξ can be evaluated to give an analytical expression for the e-h pair profiles at different depths of penetration [7]. Figure 4 shows the profiles given by the analytical expressions corresponding to Fig. 3(a) for krypton at depths of 5, 10, 15, 20, and 25 μm. The reduction of

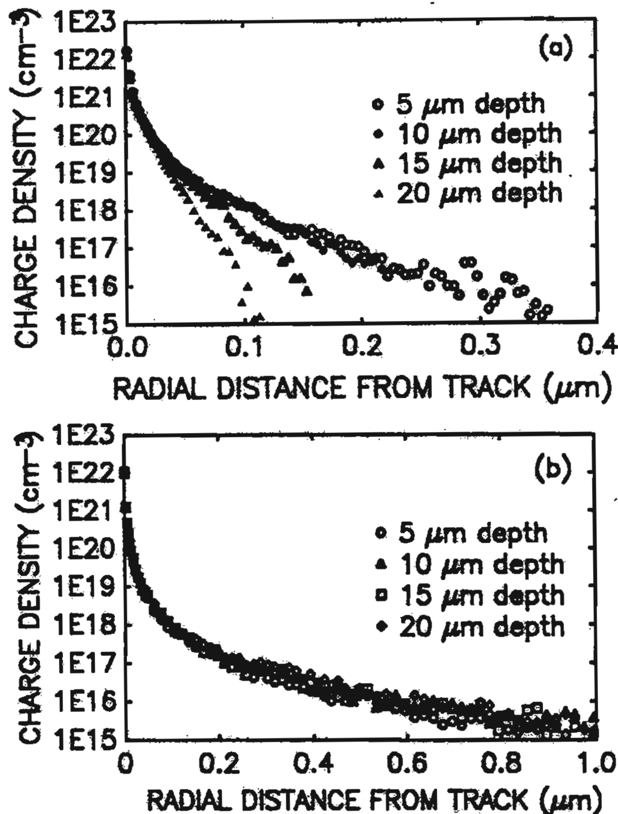

FIGURE 3. Radial volumetric charge density in silicon due to high-energy secondary electrons (initial energies > 0.5 keV) at several positions along the ion's path: (a) 270 MeV krypton, (b) 20 GeV iron.

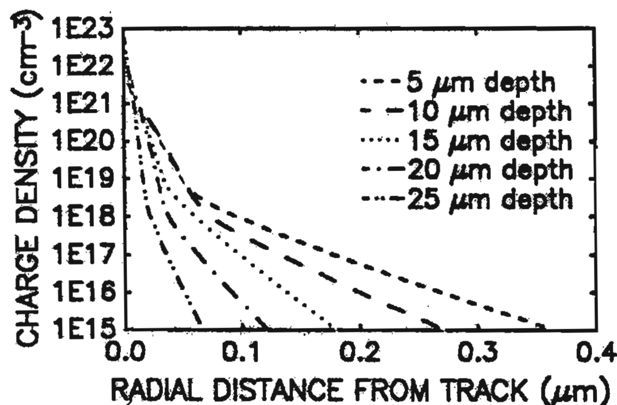

FIGURE 4. Radial volumetric charge-density profiles as a function of depth given by the analytical formula, Eq. (6). (270-MeV krypton incident on silicon)

track width as a function of depth is clear. Although peak densities exceed 10^{22} cm^{-3}, these concentrations within the core will quickly decline due to the Auger recombination of e-h pairs within the time frame of initial charge collection, as shown in Fig. 5. Simulations of charge collection during SEUs show the initial current pulse to occur between 10 and 100 ps after the ion passes [11]. Figure 5 indicates carrier concentrations will decline to values on the order of 10^{20} cm^{-3} before charge collection occurs. This value is in agreement with peak e-h pair concentrations generated during laser annealing of silicon [12].

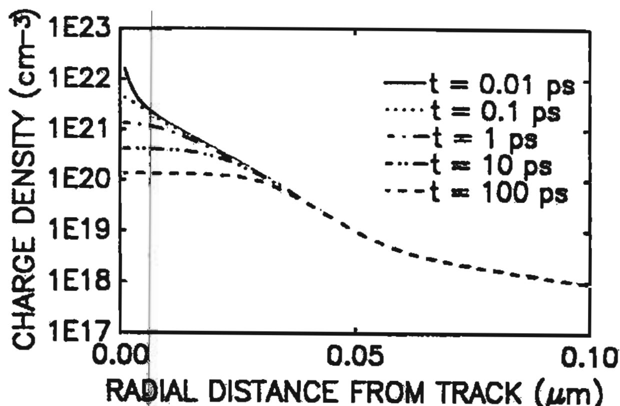

FIGURE 5. Variation of peak charge density with time due to Auger recombination of e-h pairs. (270-MeV krypton incident on silicon at a depth of 5 μm)

Evaluations of the track parameters for the argon and krypton ions studied are given in Table 1. Note that the e-folding distance of the track represented by b_2 is significantly greater than 0.1 μm in most cases.

DISCUSSION

Because of the energetic secondary electrons, typical heavy-ion track radii in silicon can be much larger than the conventionally accepted values of about 0.1 μm. Although tracks of 1 μm radius have been postulated due to diffusion processes, the time frame for this is believed to be on the order of 500 ps [4]. Our simulation has found average secondary electron slowing-down times on the order of 10^{-14} s, allowing for creation of larger initial tracks than has previously been thought. For krypton and argon ions, widely used in the cyclotron testing of SEUs, the track radius is a substantial fraction of a micron. For galactic cosmic ray particles it can exceed 0.5 μm. Experimental evidence of large track size from cosmic particles has been reported using photographic emulsions [5,13]. Our results show the radial distribution of charge density in the track is neither constant nor Gaussian as commonly believed, but agrees well with an exponential decay characteristic of high-energy penetration. Without consideration of high-energy electrons, these large track sizes and long exponential profiles would not be created.

Differences between Figs. 3(a) and 3(b) relate to the accuracy of cyclotron simulations of the space environment. Because both these heavy ions have high LETs, cyclotron testing of krypton is assumed to give effects indicative of a cosmic environment. Iron ions with energies approaching 1 GeV generate large radial concentrations of charge carriers much further from the ion path than does high-energy krypton. In addition, Fig. 3(a) shows the radial carrier profile for krypton to have decreased significantly within 15 μm of ion penetration. For cosmic iron with its much greater range, the carrier profile is much more uniform over this depth. For typical device dimensions these differing results may impact the accuracy of cyclotron simulations of SEUs in space.

As device sizes become smaller, accurate SEU simulations cannot be accomplished without giving proper consideration to the ion track size. For example, we show in Fig. 6 the calculated ratio of double- to single-bit upset for the surface layer (CMOS) case given in Fig. 1 as a function of drain separation for three values of track radii. The ratio was calculated for drains with a 10 μm x 10 μm surface

TABLE 1. Parameters for analytical track profiles.

	270 MeV Krypton			180 MeV Argon		
Depth (μm)	b_1(Å)	b_2(Å)	ϵ	b_1(Å)	b_2(Å)	ϵ
5	246	483	0.0462	384	893	0.0342
10	262	359	0.0345	325	909	0.0622
15	146	205	0.0443	268	741	0.0596
20	128	149	0.0140	232	583	0.0661
25	64	77	0.0074	200	404	0.0644
30	--	--	--	115	222	0.0913

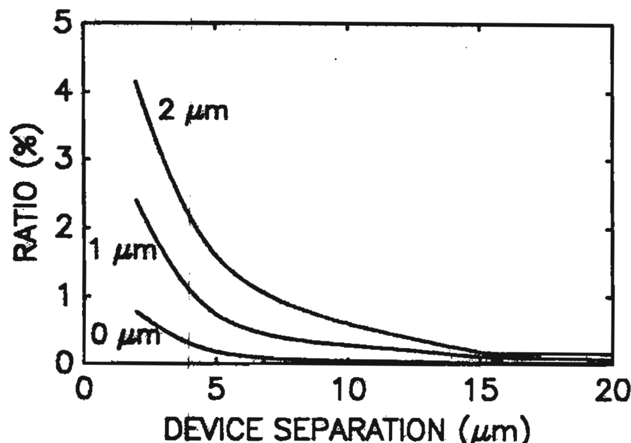

FIGURE 6. Ratio of the calculated probabilities of double- to single-bit upset for the surface layer device, assuming ion track radii of 0, 1, and 2 μm.

area and 1-μm junction depth and an isotropic flux of infinite range particles. For different assumed track radii, the solid angle representing the probability of traversing two adjacent nodes by a single track was used to evaluate the probability of double-bit upset. To calculate the ratio of double- to single-bit upsets, these probabilities were compared to the probability of the track intercepting a single node. In reference to Fig. 1, the effective depth of the junction, d_{eff}, is increased by $r_0 \sec\theta$, with r_0 the assumed track width and θ the ion angle of incidence with respect to the surface. This effective depth and 10-μm width gives each node's effective area susceptible to upset. Evaluation of the maximum solid angle over which the ion path can intersect the sensitive areas of both nodes is evaluated and compared with the probability of an ion intersecting the 10 μm x 10 μm surface area of the node, assuming an isotropic flux. The relative probability of a single-bit upset is given by:

$$\text{Single-bit upset cross section} = 4\pi ab \quad , \quad (8)$$

with a and b the surface dimensions of the node, equal to 10 μm, and 4π representing an isotropic flux of 4π steradians. The relative probability for double-bit upset is given by:

$$\text{Double-bit upset cross section} = 8\pi b d_{eff}(A_{proj}/4\pi \ell^2) \quad . \quad (9)$$

The term in parentheses represents the solid angle for intersection of both effective areas by the ion path, with ℓ half the distance of separation between the nodes and A_{proj} the effective node area projected onto

a sphere of radius ℓ. A_{proj} is given by the product of b, d_{eff}, and the ratio of surface areas of a sphere with diameter 2ℓ and a cube with width 2ℓ. An additional factor of two in Eq. (9) accounts for ions traversing in opposite directions.

As the track size approaches the micron range, this ratio becomes significant, as much as several percent for drain separations between 5 and 10 μm which is typical of current technologies. This calculation is conservative since it does not include effects of funneling. In the space environment where cosmic rays are isotropic, this finite size effect of charge tracks is probably the reason for the high multiple-bit upset rates [1,2]. Although this simplified geometrical model does not involve detailed charge collection analyses, it should give some approximation of the likelihood of double-bit upsets. Previous modeling efforts [11] showed funneling results when carrier generation exceeds the background dopant levels at the vicinity of the junction depletion layer. In our study, track widths correspond to a region where carrier concentrations are above background dopant levels. Funneling will likely occur with these tracks, although we have not explicitly addressed this issue.

Another evaluation of the ratio of double- to single-bit upsets was made for a buried layer, bipolar collector-to-substrate junction (Fig. 7). The sensitive junction node is assumed to have dimensions of 50 μm x 20 μm lateral area and 2-μm junction depth. Calculations are handled as before except for the different device dimensions and the fact that effective depth must include the term $2r_0\sec\theta$ rather than $r_0\sec\theta$, to account for ion tracks passing both above and below the node in question. The calculated ratio of double- to single-bit upsets for this device as a function of drain separation is given in Fig. 8. With the depth of the sensitive node twice that of the surface layer (CMOS) case, the probability of double-bit upsets is also greater and becomes very significant as device separations decrease to 5 μm or less.

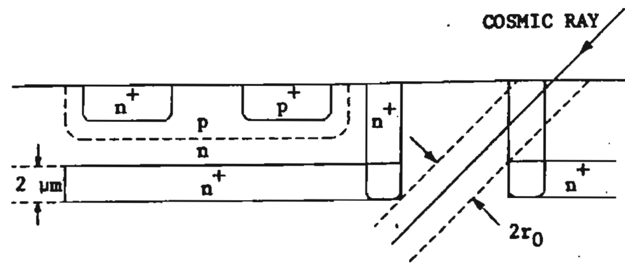

FIGURE 7. Schematic of a buried layer device with oblique incident angle of cosmic ray causing double-bit upset.

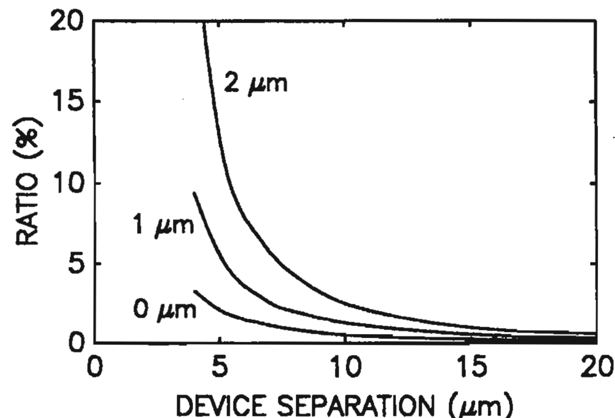

FIGURE 8. Ratio of the calculated probabilities of double- to single-bit upset for the buried layer device, assuming ion track radii of 0, 1, and 2 μm.

CONCLUSIONS

High-energy secondary electrons created by heavy ions are expected to cause a considerable widening of the initial charge tracks compared with previous assumptions. The wider charge tracks evaluated in this study better account for experimentally reported double-bit upset rates in space than do previous assumptions of track widths. The approach used in this study to calculate double-bit upset probabilities shows fair agreement with experiment for track radii between 0.5 and 1 μm. Charge tracks generated by typical cyclotron SEU-simulation particles, such as argon and krypton, are in general narrower than typical cosmic particle tracks. In addition, the cyclotron particles are attenuated faster and have less uniform track generation with depth than the cosmic particles. These differences may make accurate quantitative evaluations difficult when using cyclotron particles for simulation of cosmic particle-induced phenomena.

REFERENCES

1. J. B. Blake and R. Mandel, IEEE Trans. Nucl. Sci., vol. NS-33, No. 6, pp. 1616-1619, Dec. 1986; and private communication with J. B. Blake.

2. R. J. Moore, "TDRSS SEU Operational Overview and Corrective Action," presented at the 5th Annual Symposium on Single Event Effects, Los Angeles, CA, April 7-8, 1987.

3. H. L. Grubin, et al., IEEE Trans. Nucl. Sci., vol. NS-31, No. 6, pp. 1161-1166, Dec. 1984.

4. G. C. Messenger, IEEE Trans. Nucl. Sci., vol. NS-29, No. 6, pp. 2024-2031, Dec. 1982.

5. E. J. Kobetich and R. Katz, Phys. Rev., vol. 170, pp. 405-411, June 1968.

6. P. Chou and N. M. Ghoniem, J. Nucl. Mater., vol. 117, pp. 55-63, July 1983.

7. R. C. Martin and N. M. Ghoniem, "Coupled Ion-Electron Transport in Semiconductors," UCLA Report No. UCLA-ENG-8708/PPG-1024, March 1987.

8. H. J. Fitting and J. Reinhardt, Phys. Status Solidi A, vol. 88, pp. 245-259, March 1985.

9. A. Ya. Vyatskin and V. V. Trunev, Radiotekh. Elektron., vol. 12, No. 9, pp. 1636-1641, 1967.

10. C. J. Tung et al., "Inverse Mean Free Path, Stopping Power, CSDA Range, and Straggling in Silicon and Silicon Dioxide for Electrons of Energy $\leq$ 10 keV," Report No. RADC-TR-76-125, April 1976.

11. C.-M. Hsieh, P. C. Murley, and R. R. O'Brien, IEEE Trans. Electron Devices, vol. ED-30, No. 6, pp. 686-693, June 1983.

12. A. L. Smirl, in Cohesive Properties of Semiconductors under Laser Irradiation, ed. L. D. Laude, The Hague: Martinus Nijhoff Publishers, 1983, pp. 348-390.

13. W. A. Kolasinski et al., IEEE Trans. Nucl. Sci., vol. NS-26, No. 6, pp. 5087-5091, Dec. 1979.